



Original article

Synthesis, radiolabeling and evaluation of novel 4-oxo-quinoline derivatives as PET tracers for imaging cannabinoid type 2 receptor



Roger Slavik^a, Adrienne Müller Herde^a, Daniel Bieri^a, Markus Weber^b, Roger Schibli^a, Stefanie D. Krämer^a, Simon M. Ametamey^{a,*}, Linjing Mu^{c,*}

^a Institute of Pharmaceutical Sciences, ETH Zürich, 8093, Zürich, Switzerland

^b Neuromuscular Diseases Unit/ALS Clinic, Kantonsspital St. Gallen, 9007, St. Gallen, Switzerland

^c Department of Nuclear Medicine, University Hospital Zürich, 8091, Zürich, Switzerland

ARTICLE INFO

Article history:

Received 29 October 2014

Received in revised form

10 January 2015

Accepted 12 January 2015

Available online 13 January 2015

Keywords:

Cannabinoid receptor type 2

Neuroinflammation

Radiolabeling

Autoradiography

Positron emission tomography

ABSTRACT

Our goal is to develop a highly specific and selective PET brain tracer for imaging CB2 expression in patients with neuroinflammatory diseases. Based on our previous findings on a carbon-11 labeled 4-oxo-quinoline structure, designated KD2, further structural optimizations were performed, which led to the discovery of *N*-(1-adamantyl)-1-(2-ethoxyethyl)-8-methoxy-4-oxo-1,4-dihydroquinoline-3-carboxamide (**RS-016**). Compared to KD2, **RS-016** exhibits a higher binding affinity towards CB2 ($K_i = 0.7$ nM) with a selectivity over CB1 of >10,000 and lower lipophilicity ($\log D_{7.4} = 2.78$). [¹¹C]**RS-016** was obtained in ≥99% radiochemical purity and up to 850 GBq/μmol specific radioactivity at the end of synthesis. *In vitro* autoradiography on rodent spleen tissue showed high specific binding to CB2. [¹¹C]**RS-016** was stable *in vitro* in rodent and human plasma over 40 min, whereas 47% intact compound was found *in vivo* in rat blood plasma 20 min post injection (p.i.). High specific binding to CB2 was observed in murine spleen tissues and postmortem ALS patient spinal cord tissues *in vitro* autoradiography, *ex vivo* biodistribution data confirmed the high and specific uptake of [¹¹C]**RS-016** in spleen region in rats. *In vivo* specificity of [¹¹C]**RS-016** could also be shown in brain by PET imaging using a murine neuroinflammation model, which has higher CB2 receptor expression level in the brain induced by lipopolysaccharide (LPS) application.

© 2015 Elsevier Masson SAS. All rights reserved.

1. Introduction

The endocannabinoid system is activated on demand to preserve cell homeostasis in both periphery and brain. Its receptors, cannabinoid receptor 1 and 2 (CB1 and CB2), were first identified in 1990 [1] and 1993 [2], respectively. Both are G_{i/o}-protein coupled receptors with seven transmembrane helices. CB1 receptors are mainly expressed on neurons in cortex, hippocampus, amygdala, basal ganglia and cerebellum, but to a less extent in peripheral tissues [3,4]. CB2 receptors are abundant on immune cells such as B-lymphocytes, natural killer cells or monocytes [2] and have very

low concentration in brain tissue under basal conditions [5–7]; however, it is up-regulated in cerebellum, cortex and brainstem in pathological conditions such as in multiple sclerosis, traumatic brain injury, HIV-induced encephalitis, Alzheimer's disease, Parkinson's disease and Huntington's disease [8,9]. Upregulation of CB2 in spinal cord was detected in a mouse model of Amyotrophic lateral sclerosis (ALS) as well as in human spinal cord tissues from ALS patients [10,11]. ALS is a progressive neurodegenerative disorder affecting both upper and lower motor neurons in spinal cord, brain stem and motor cortex. Of all ALS cases, 90–95% occur in a sporadic form, whereas 5–10% are inheritable familial cases, partly due to mutations in superoxide dismutase 1 gene (SOD1) [12]. Patients suffer from high symptom burdens including pain, fatigue, dyspnea, and sialorrhoea and the average life span after diagnosis is about three years. There is no effective treatment available today, although a lot of progress has been made in this direction over the past few years (for review article see Ref. [13]).

Non-invasive imaging of CB2 upregulation *via* Positron emission

Abbreviations: ALS, Amyotrophic lateral sclerosis; HBTU, O-(Benzotriazol-1-yl)-N,N,N',N'-tetramethyluronium hexafluorophosphate; hCB2, human cannabinoid receptor type 2; PET, Positron emission tomography.

* Corresponding author. NUK D2, 8091, Zürich, Switzerland.

** Corresponding author. HCI H427, 8093, Zürich, Switzerland.

E-mail addresses: simon.ametamey@pharma.ethz.ch (S.M. Ametamey), linjing.mu@usz.ch (L. Mu).

tomography (PET) could help to understand pathology that involves CB2 and explore the role and importance of CB2 in (neuro) inflammation and to evaluate the therapeutic value of new CB2-related drugs [14–16].

Several CB2 PET radioligands have been reported by different groups (Fig. 1). Among these, [^{11}C]NE40 is the only CB2 radioligand which has been evaluated in healthy volunteers [17]. Expected uptake in lymphoid tissue and appropriate brain kinetics were observed. Recently, we evaluated [^{11}C]KD2 as an imaging agent for CB2 receptor [18], and it is not optimal yet probably due to its high lipophilicity. This prompted us to search for suitable candidate compounds that retain the high affinity and selectivity profile of KD2 for CB2 but show reduced lipophilicity. We report herein the design and synthesis of a series of novel 4-oxo-quinoline derivatives based on the lead structure of KD2. Structure–activity relationship (SAR) studies revealed compound **RS-016** (Scheme 1) as a very promising ligand, therefore, **RS-016** was selected for radiolabeling with carbon-11 and its utility as an imaging agent was examined *in vitro/in vivo* studies.

2. Results

2.1. Chemistry

Novel derivatives based on the structure of KD2 were synthesized starting from commercially available anisidine and diethyl 2-(ethoxymethylene)malonate as depicted in Scheme 1. Compound **2** was prepared *via* the Gould–Jacobs reaction and subsequent benzannulation at high temperatures as previously described [18,25]. *N*-alkylation of quinolone ester **2** afforded compounds **3a–c** under basic conditions in 83–96% yields. Free quinoline acids **4a–c** were obtained by saponification of their corresponding ethyl esters with 10% sodium hydroxide. Reacting of **4a–c** with different amines using HBTU as the coupling reagent afforded to the eight final compounds **RS-005**, **RS-006**, **RS-007**, **RS-008**, **RS-011**, **RS-016**, **RS-022** and **RS-028** in 69–92% yield after the purification by flash column chromatography.

3-Hydroxy-1-aminoadamantane (**5**), which was used for the synthesis of compound **RS-028**, was obtained by nitration of 1-aminoadamantane using 65% nitric acid in conc. sulfuric acid followed by hydrolysis using KOH (Scheme 2) [26].

2.2. Structure–activity relationship (SAR) study

Eight novel compounds were submitted to the SAR studies for their binding affinities towards CB2 and selectivities over CB1. *In vitro* competitive binding assays were performed with human CB1 and CB2 membranes using [^3H]-CP-55940, a non-specific CB agonist, as the radioligand. All compounds exhibited excellent selectivity over CB1 and K_i values towards the CB2 receptor ranged from 0.7 to 750 nM (Fig. 2, Table 1). Pasquini et al. [25] reported that a class of 4-quinolone-3-carboxamides with pentyl group in the R_1 position (Fig. 2) showed high binding affinities towards CB2, we found that replacing pentyl to butyl group in the R_1 position as shown in **RS-005** had no significant impact on its binding affinity towards CB2, and with a positive influence on its lipophilicity. A K_i value of 3.3 nM was obtained for the butyl derivative **RS-005** whereas for the pentyl derivative KD2 a value of 1.7 nM was obtained. Keeping the shorter butyl side chain and introducing less bulky groups such as *tert*-butyl, cyclopentyl, methylcyclopropyl in the R_2 position gave rise to three novel compounds **RS-006**, **RS-007** and **RS-008**, respectively. Replacement of the adamantyl moiety with a smaller but still bulky *tert*-butyl moiety resulted in an approximately 26 times less lipophilic compound **RS-006** based on the calculated clogP values of 2.87 compared to **RS-005** (clogP 4.29), while its K_i value was still at the level of single digit nanomolar range. In general, variation of the substituents in the R_2 position could influence both the lipophilicity and their binding affinities. As introduction of a fluorine atom is of high interest for imaging agent, therefore, **RS-011** was synthesized with a fluoroethyl side chain in the R_1 position and keeping the *tert*-butyl group in R_2 position, however, it showed the weakest binding affinity among all the tested compounds. The reason might be due to the relative short alkyl chain length in the R_1 position of **RS-011**

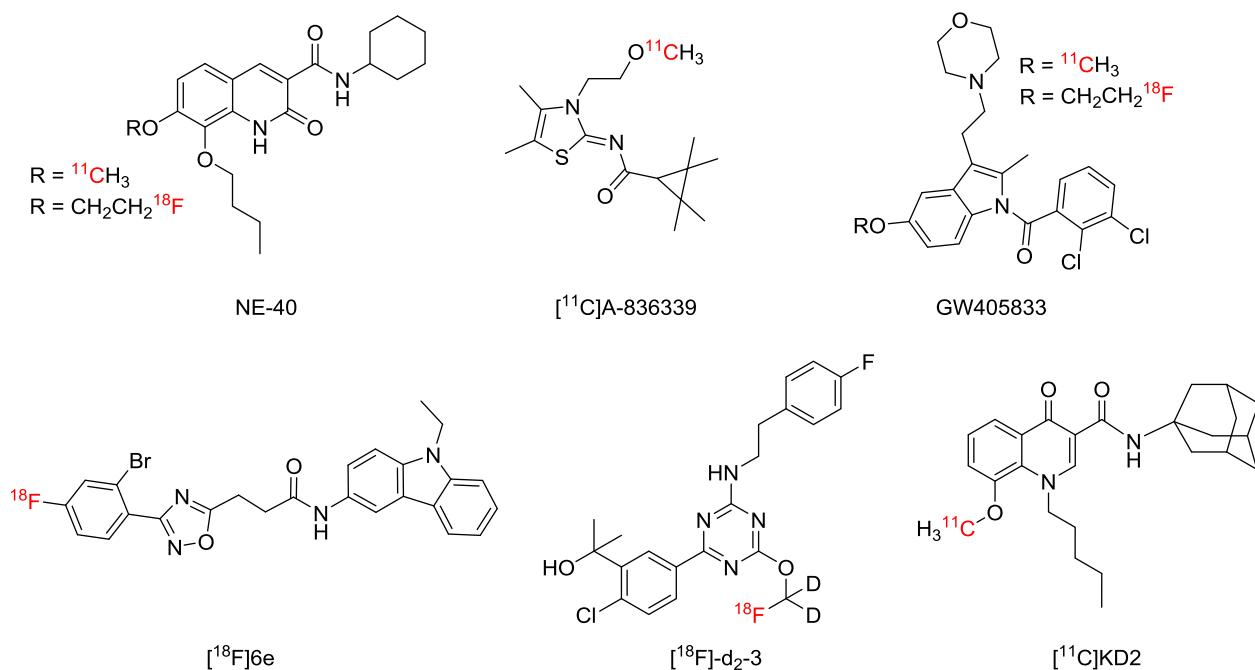
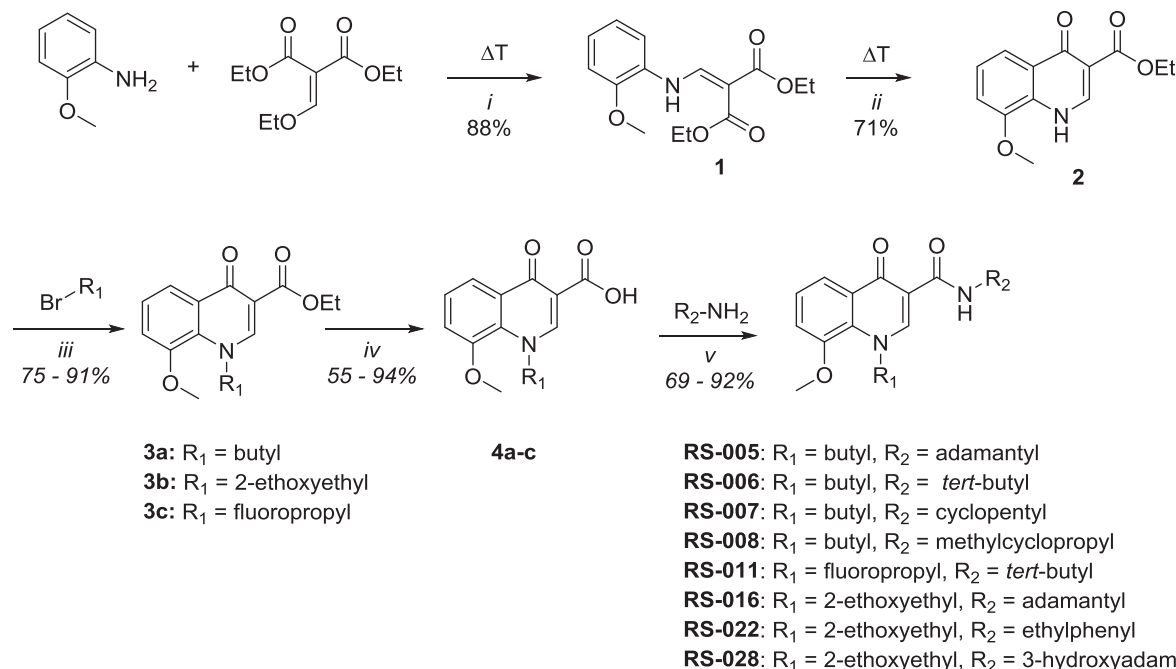
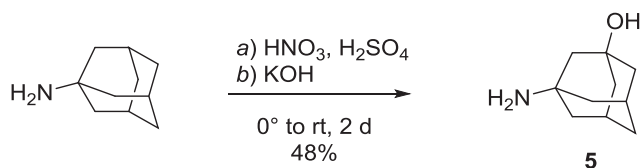


Fig. 1. Representative CB2 PET ligands NE-40 [19], [^{11}C]A-836339 [20], GW405833 [21,22], [^{18}F]6e [23], [^{18}F]d₂-3 [24] and [^{11}C]KD2 [18].



Scheme 1. Synthesis towards novel KD2 derivatives. Reagents and Conditions: (i) 110 °C, 1 h, (ii) diphenylether, 250 °C, 1 h, (t, iii) K₂CO₃, DMF, 90 °C, 4 h, (iv) 10% NaOH, reflux, 3.5 h, (v) DIPEA, HBTU, DMF, r4 h.



Scheme 2. Synthesis of 3-hydroxyaminoadamantane.

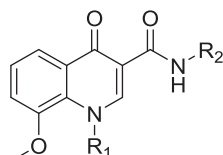


Fig. 2. Novel 4-oxo-quinoline structures as potential CB2 brain PET tracers.

compared to other tested compounds. Further structural modifications in the R₁ position with a small PEG group and adamantyl substituent in the R₂ position as shown in compound **RS-016** resulted the highest binding affinity to CB2 (0.7 nM) among all the newly synthesized compounds and an optimal clogP value of 3.0 (Table 1). Hydroxylation of **RS-016** on adamantyl moiety led to compound **RS-028**, which displayed a similar K_i value of 0.8 nM as **RS-016** (K_i 0.7 nM). However, its low lipophilicity (clogP 1.62) and relative large polar surface area of 88 Å² could have an adverse effect on the blood–brain barrier penetration. Therefore, **RS-016** (clogP 3.0; tPSA = 68 Å²) was selected for radiolabeling with C-11 and further *in vitro/in vivo* evaluations. There is no direct correlation between the compounds' lipophilicity and their binding affinities towards CB2 based on our current results.

2.3. Radiosynthesis

Compound **6**, which served as the precursor for the

radiosynthesis, was obtained by treatment of reference compound **RS-016** with lithium chloride (Scheme 3) in 20% yield after HPLC purification. The radiosynthesis of [¹¹C]**RS-016** was accomplished in a one-step procedure by *O*-methylation of the cesium salt of **6** using [¹¹C]CH₃I (Scheme 3) in up to 33% radiochemical yield (decay corrected). The radiolabeled product was purified by semi-preparative HPLC and obtained in ≥99% radiochemical and chemical purity. [¹¹C]**RS-016** was formulated in 5% ethanol in water for all *in vitro/in vivo* experiments. The specific radioactivity was in the range of 545 ± 154 GBq/μmol with a total radioactivity of 4.42 ± 1.05 GBq at the end of synthesis (n = 39). The total synthesis time from end of bombardment was approximately 35 min.

2.4. In vitro characterization of [¹¹C]**RS-016**

The *in vitro* stability of [¹¹C]**RS-016** in rodent and human plasma was assessed over a time course of 40 min. No radioactive degradation products of [¹¹C]**RS-016** were observed. The LogD value at physiological pH 7.4 was 2.78 ± 0.04 (n = 5), which is within the optimal lipophilicity range for brain-penetrating compounds [27,28]. Autoradiography experiments on rodent spleen tissues demonstrated that [¹¹C]**RS-016** exhibits high specific binding to CB2 using the highly selective CB2 ligand GW405833 (K_i towards hCB2 3.9 nM; hCB1 4772 nM [29]) as a blocker (Fig. 3). To evaluate the potential of [¹¹C]**RS-016** for imaging ALS, post mortem spinal cord tissues from ALS patients were used in autoradiography experiments. High accumulation of [¹¹C]**RS-016** was observed in both cervical and lumbar spinal cord sections similar to our previous studies with [¹¹C]KD2 [16].

2.5. In vivo characterization of [¹¹C]**RS-016** in rats

To study the metabolic stability of [¹¹C]**RS-016** *in vivo*, the radiotracer was injected intravenously into Wistar rats and the blood samples were collected at different time points after tracer injection. The animals were sacrificed by decapitation at 20 min p.i.

Table 1

Binding affinities for novel KD2 derivatives. The data are expressed as the mean \pm SEM of $n = 3$ independent experiments. ClogP as calculated lipophilicity by ChemDraw (CambridgeSoft).

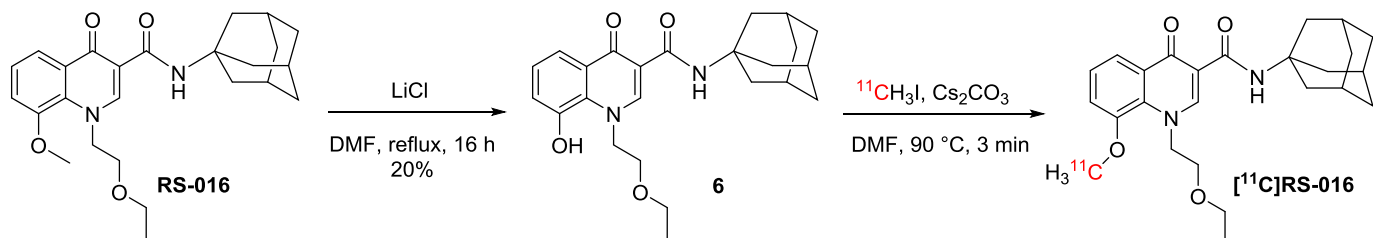
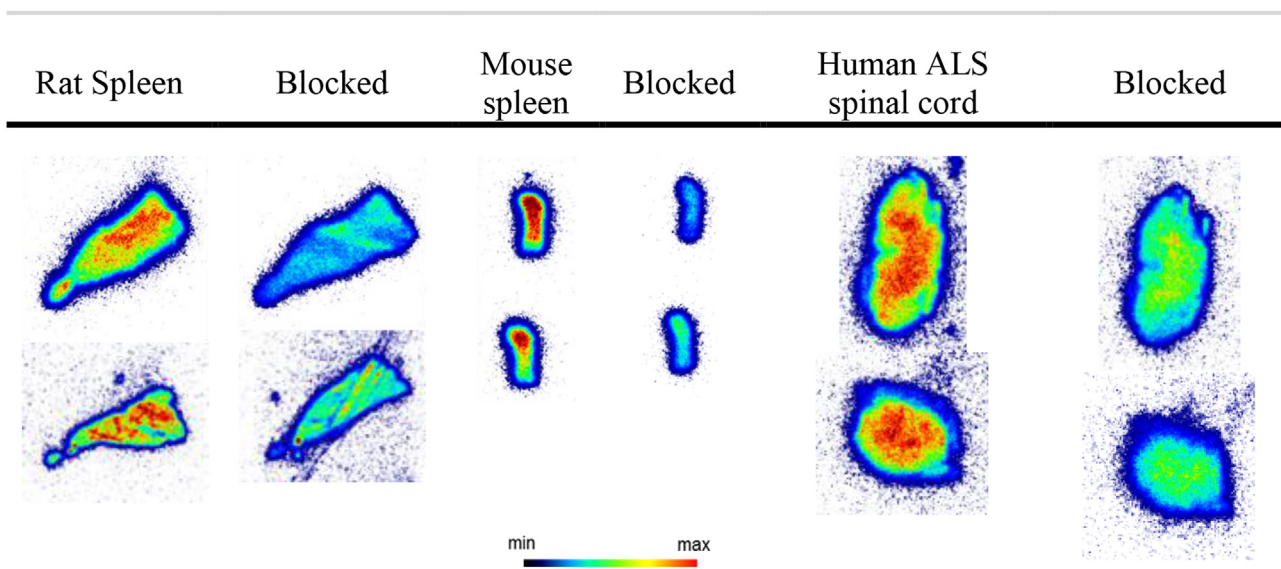
Compd	R ₁	R ₂	clogP	K _i CB ₂ [nM]	K _i CB ₁ [nM]
KD-2			4.82	1.7 \pm 2.0	>10,000
RS-005			4.29	3.3 \pm 0.2	>10,000
RS-006			2.87	8.2 \pm 5.5	>10,000
RS-007			3.10	19.7 \pm 8.8	>10,000
RS-008			2.60	78.8 \pm 33.1	>10,000
RS-011			1.76	750 \pm 780	>10,000
RS-016			3.0	0.7 \pm 0.6	>10,000
RS-022			2.46	360 \pm 240	>10,000
RS-028			1.62	0.8 \pm 0.8	>10,000

Table 2

Biodistribution in rats. Animals were sacrificed at 15 min after injection of [¹¹C]RS-016; 5–10 MBq (0.01–0.02 nmol, $n = 3$) for baseline and (6–8 MBq, $n = 3$) for blocking conditions.

Tissue	Baseline [norm. %ID/g]	Blocked [norm. %ID/g]
Spleen	0.284 \pm 0.029	0.062 \pm 0.011
Liver	0.505 \pm 0.033	0.380 \pm 0.058
Kidneys	0.122 \pm 0.010	0.134 \pm 0.026
Adrenal gland	0.216 \pm 0.013	0.262 \pm 0.017
Lung	0.088 \pm 0.007	0.075 \pm 0.011
Bone	0.046 \pm 0.004	0.039 \pm 0.003
Heart	0.080 \pm 0.004	0.091 \pm 0.014
Fat	0.050 \pm 0.014	0.053 \pm 0.013
Small intestine	0.924 \pm 0.260	0.425 \pm 0.295
Testis	0.033 \pm 0.005	0.034 \pm 0.003
Blood	0.044 \pm 0.004	0.030 \pm 0.007
Thyroid gland	0.077 \pm 0.007	0.064 \pm 0.016
Urine	0.060 \pm 0.028	0.080 \pm 0.015
Muscle	0.065 \pm 0.005	0.071 \pm 0.003
Pancreas	0.110 \pm 0.005	0.113 \pm 0.005
Skin	0.050 \pm 0.008	0.057 \pm 0.010
Brain	0.025 \pm 0.004	0.028 \pm 0.001

than [¹¹C]RS-016, was detected. The percentage of parent tracer radioactivity decreased to 72% at 5 min p.i., 55% at 10 min p.i. and 47% at 20 min p.i. No parent compound could be detected in urine

**Scheme 3.** Synthesis of precursor **6** and radiosynthesis of [¹¹C]RS-016.**Fig. 3.** *In vitro* autoradiography with 0.4 nM [¹¹C]RS-016 and 5 μ M GW405833 as blocking agent showing specific binding in rodent spleen tissue and human post mortem cervical (top) and lumbar (bottom) spinal cord tissue from two different ALS patients.

and urine and spleen tissue were collected. In all blood plasma samples, only one radiometabolite, which was more hydrophilic

sample after 20 min p.i., while in spleen sample, 81% radioactivity was intact parent compound.

The results of the biodistribution study in rats are shown in Table 2. The highest concentration of [^{11}C]RS-016 at 15 min after injection were found in small intestine, liver and spleen, followed by adrenal gland, kidneys and pancreas (Table 2). Radioactivity uptake in the intestine and liver was much higher than in the kidneys, suggesting a preponderance of hepatobiliary elimination over renal excretion. Concentrations in brain tissue were very low as expected from low CB2 expression levels under healthy conditions [5]. The spleen uptake was 0.284 ± 0.029 norm. %ID/g at 15 min p.i., which was reduced by 78% under blocking conditions with 1.5 mg/kg GW405833. This is in line with the high physiological expression level of CB2 in spleen tissue [30], indicating binding specificity of [^{11}C]RS-016 to CB2.

2.6. CB2 gene expression levels after LPS treatment in mice

The suitability of [^{11}C]RS-016 as an imaging agent in neuro-inflammatory and neurodegenerative diseases was evaluated in a LPS mouse model of neuroinflammation [31]. To address the question to which extent CB2 gene expression is altered after LPS application, we measured CB2 mRNA levels in the brain and spleen of mice (Fig. 4). In the brain, significant upregulation of CB2 was found at 5 days after injection of 10 mg/kg LPS. Gene expression of CB2 was 9.5-fold higher in LPS-treated mice than in vehicle-treated mice (0 mg/kg LPS). After 3 days, a two-fold increased CB2 expression was found after injection of 10 mg/kg LPS. Applications of 5 mg/kg LPS did not change CB2 expression levels in the brain. In spleen tissue, CB2 levels were increased at 3 and 5 days after 10 mg/kg LPS injection, but not at 5 mg/kg LPS, compared to vehicle.

2.7. Imaging of CB2 upregulation in mouse brain after LPS treatment

The upregulated CB2 receptor expression in mouse brain 5 days after 10 mg/kg LPS application was verified by *in vitro* autoradiography (Fig. 5) using [^{11}C]RS-016. A higher radioactivity accumulation of [^{11}C]RS-016 was observed in the brain tissue of LPS-treated mice compared to vehicle-treated mice. Co-incubation of the brain sections with 0.2 nM [^{11}C]RS-016 and excess amount of GW405833 (5 μM) led to a significant reduction of radioactivity binding, indicating specificity of [^{11}C]RS-016 for CB2.

To investigate the performance of [^{11}C]RS-016 *in vivo*, dynamic brain PET scans were performed with this mouse model. Time-activity curves (TACs) of mouse whole brain, cortex, hippocampus and cerebellum are shown in Fig. 6. Increased [^{11}C]RS-016 accumulation was found in all brain regions after LPS treatment

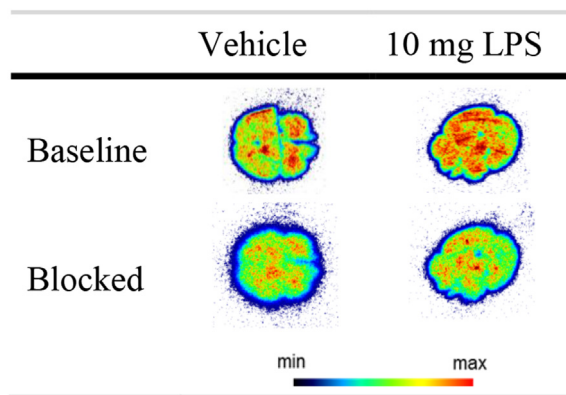


Fig. 5. *In vitro* autoradiography on mouse brain Sections 5 days after treatment with vehicle (0 mg/kg LPS) or 10 mg/kg LPS using 0.2 nM [^{11}C]RS-016 and with 5 μM GW405833 as the blocking agent.

compared to vehicle group (0 mg/kg LPS). This accumulation was reduced to levels of the vehicle group in all brain regions after blockade with 2 mg/kg GW405833.

3. Discussion

CB2 plays an important – yet not fully understood – role in neuroinflammatory conditions. A specific CB2 PET tracer would help to gain deeper insight into the pathophysiology of different diseases on a molecular basis and will allow the monitoring of disease progression and therapeutic outcome in the clinic. Our group recently reported a specific CB2 PET tracer [^{11}C]KD2, which shows overall good properties, but exhibits high non-specific binding and very low free fraction f_u in plasma, in agreement with its high lipophilicity. Therefore, an optimization was necessary based on the structural motif of KD2. *N*-alkylation of the quinolone moiety allowed the introduction of different alkyl moieties that provide the possibility to change its lipophilicity. Further structural variations were made *via* the amide bond formation with different amines. In general, the syntheses of all compounds were straightforward with good yields. HPLC purification was necessary for obtaining pure product precursor compound 6. All of the novel KD2 derivatives presented in this paper showed high selectivity against CB1 and lower calculated clogP values than the reference compound KD2. Their lipophilicities were reduced successfully by introduction of smaller alkyl side chains or substitution with an ether group in the R1 position, whereas binding affinities towards

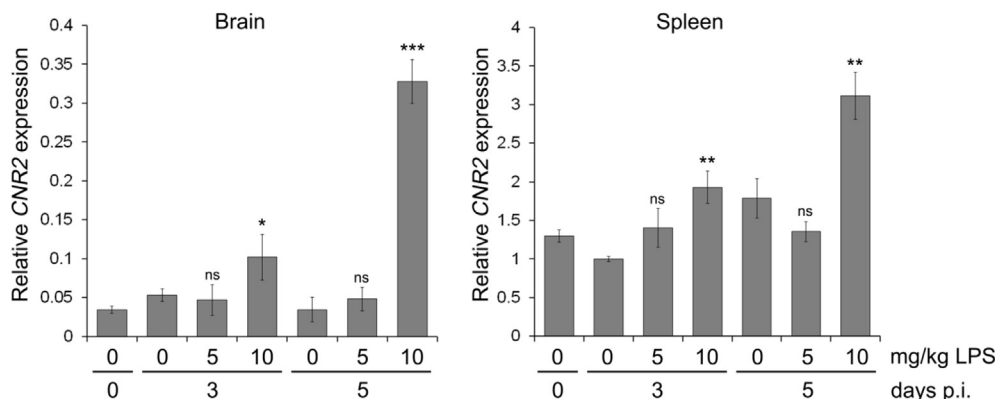


Fig. 4. Gene expression levels of murine CB2 in whole brain and spleen at 0, 3 and 5 day post ip injection of 0, 5 or 10 mg/kg LPS. * $P < 0.05$; ** $P < 0.01$; *** $P < 0.001$; ns, not significant relative to 0 mg/kg LPS of the respective day.

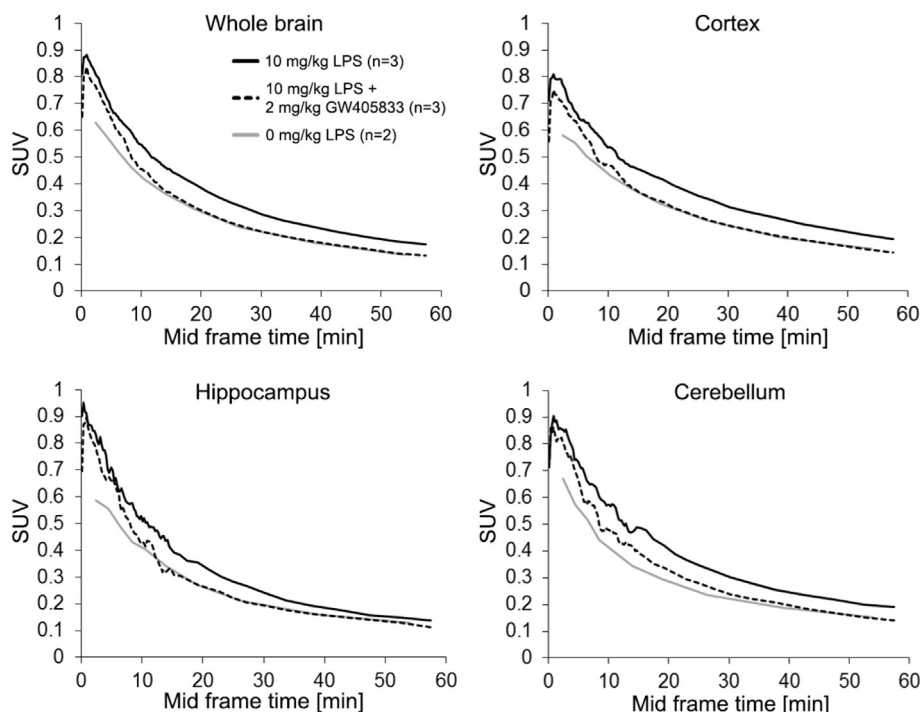


Fig. 6. Averaged time–activity curves of [^{11}C]RS-016 in whole brain, cortex, hippocampus, and cerebellum 5 days after application of 0 or 10 mg/kg LPS (solid lines, standard deviations < 17%) and under blocking conditions with 2 mg/kg GW405833 30 min prior injection of [^{11}C]RS-016 (dashed line, standard deviations < 6%), $n = 2 - 3$. Values within 5–40 min p.i. of LPS-treated group and blockade group are significant different ($P < 0.05$) for the depicted brain regions.

CB2 were maintained in single digit nanomolar range. Decreasing the size of the amide substituents in the R2 position had similar favorable effects. Compound **RS-016** displayed highest binding affinity towards CB2 ($K_i = 0.7$ nM) and was therefore selected for further evaluation as potential CB2 PET tracer.

Compared to the lead compound KD2 [18], **RS-016** exhibits more than three times lower $\log D_{7.4}$ value than KD2 (2.78 vs 3.29) and 2.4-fold higher binding affinity to hCB2 (K_i : 0.7 nM vs. 1.7 nM). We tried to estimate the non-specific binding of [^{11}C]RS-016 compared to [^{11}C]KD2 to CB2-positive spleen tissue by *in vitro* autoradiography studies. A lower non-specific binding for [^{11}C]RS-016 than [^{11}C]KD2 was found when visually comparing the intensities of radioactivity signals on the autoradiograms under similar experimental conditions. Radioactivity accumulation of [^{11}C]RS-016 in the rat brain was low as indicated in *ex vivo* biodistribution experiments at 15 min p.i., which is in line with the low CB2 expression levels under healthy conditions [5] and in addition might be due to low blood–brain barrier penetration of compound [^{11}C]RS-016. Further experiment was planned to verify this issue. The utility of the tracer for monitoring neuroinflammation conditions was evaluated in a LPS mouse model according to published procedures from Horti et al. [20], using 10 mg/kg LPS instead of 5 mg/kg. Higher brain uptake was demonstrated in LPS-treated mice compared to vehicle-treated mice and its specificity towards CB2 was demonstrated in blockade studies both *in vitro* and *in vivo*.

4. Conclusion

We have successfully synthesized a series of 4-oxo-quinoline derivatives with nanomolar affinity towards the CB2 and excellent selectivity over CB1.

A robust and reliable radiosynthetic procedure was established for the most promising compound **RS-016** and afforded the desired product [^{11}C]RS-016 in high specific activity up to 850 GBq/ μmol ,

and radiochemical purity of $\geq 99\%$ at the end of synthesis. The $\log D_{7.4}$ value of 2.74 is within the range of an optimal lipophilicity for brain penetrating compounds. Furthermore, it outperforms the previously reported lead compound [^{11}C]KD2 in binding affinity towards CB2 and lower non-specific binding. High specific binding to CB2 was observed in murine spleen and post mortem ALS patient spinal cord tissues. In line with the *in vitro* autoradiography results, *ex vivo* biodistribution data confirmed the high and specific uptake of [^{11}C]RS-016 in spleen region in rats.

The preclinical data on [^{11}C]RS-016 indicate that this new radioligand is a promising radiotracer for imaging CB2 in humans. Further work is currently ongoing to evaluate the usefulness of [^{11}C]RS-016 in other animal models of neuroinflammation.

5. Experimental section

5.1. General

All reagents and solvents were purchased from Sigma–Aldrich Chemie GmbH (Germany), Merck (Germany), Acros Organics (Belgium), ABCR GmbH (Germany) or Fluka (Switzerland). All chemicals were used as supplied without further purification. Synthesized compounds were $>95\%$ in purity determined by analytical HPLC method on an Agilent HPLC system. ^1H and ^{13}C NMR spectra were obtained on a Bruker Avance FT-NMR spectrometer (400 MHz). Chemical shifts are given in delta (δ) units, in ppm relative to tetramethylsilane (TMS, 0 ppm). Multiplicities in the ^1H NMR spectra are described as: s = singlet, d = doublet, t = triplet, q = quartet, m = multiplet, br = broad peak. Coupling constants (J) are reported in Hz. High resolution mass spectrometry (HRMS) was performed on a Bruker's maXis (ESI-Qq-TOF-MS) spectrometer (Bruker Daltonik GmbH, Germany) and are given in m/z . ClogP values were calculated using the CambridgeSoft Software ChemDraw 13.0 (PerkinElmer, Massachusetts). Preparative

HPLC was performed with a Merck-Hitachi L7150 pump system and an Ultimate XB-C18 column (150 × 21.2 mm, 5 μm). For purification of radiolabeled product, a semi-preparative Merck-Hitachi L2130 HPLC system equipped with a radiation detector VRM 202 (Veestra Instrument, Joure, Netherlands) was used with a Waters Symmetry C8 Prep Column (50 × 7.8 mm, 100 Å, 5 μm) and an isocratic solvent system 0.1% H₃PO₄ in H₂O (30%) and CH₃CN (70%) at a flow rate of 4 mL/min. For product analysis, an analytical Agilent 1100 series HPLC system, equipped with UV multiwavelength detector and a GabiStar radiodetector (Raytest) was used with an ACE C18-AR column (50 × 4.6 mm, 3 μm) with the following conditions: 0.1% TFA in H₂O (solvent A), CH₃CN (solvent B); 0.0–3.0 min, 30% B; 3.1–13.0 min, 30–95% B; 13.1–15 min, 95% B at a flow rate of 1 mL/min.

5.2. Animals

Animal care and experiments were conducted in accordance with Swiss Animal Welfare legislation and were approved by the Veterinary Office of Canton Zurich, Switzerland. Five-week-old male Wistar rats and five-week old male CD-1 mice were supplied by Charles River (Sulzberg, Germany). As a model of neuroinflammation, which is described in the literature [31], six CD-1 male mice were injected ip (100–150 μL) with 10 mg/kg lipopolysaccharide (LPS), *Escherichia coli* strain O111:B4, or vehicle (saline) 5 days prior to PET.

5.3. Chemistry

5.3.1. Synthesis of diethyl 2-(((2-methoxyphenyl)amino)methylene)malonate (**1**)

A mixture of 2-anisidine (6.36 g, 51.6 mmol) and diethyl 2-(ethoxymethylene)malonate (11.17 g, 51.6 mmol) was heated at 110 °C for 1 h. After cooling to rt, the crude mixture was then recrystallized from hexane (50 mL) to give **1** in 88% yield. ¹H NMR (400 MHz, CDCl₃): δ 11.12 (d, *J* = 14.0 Hz, 1H), 8.57 (d, *J* = 14.0 Hz, 1H), 7.25 (dd, *J*₁ = 1.4 Hz, *J*₂ = 8.0 Hz, 1H), 7.12–7.08 (m, 1H), 7.01–6.93 (m, 2H), 4.33 (q, *J* = 7.1 Hz, 2H), 4.25 (q, *J* = 7.1 Hz, 2H), 3.94 (s, 3H), 1.38 (t, *J* = 7.1 Hz, 3H), 1.33 (t, *J* = 7.1 Hz, 3H). ¹³C NMR (100 MHz, CDCl₃): δ 168.5, 166.0, 150.4, 148.9, 128.8, 124.8, 121.2, 119.1, 114.3, 111.2, 93.8, 60.3, 60.0, 55.9, 14.4. HRMS calcd for C₁₅H₁₉NNaO₅ 316.1155, found 316.1164.

5.3.2. Synthesis of ethyl 8-methoxy-4-oxo-1,4-dihydroquinoline-3-carboxylate (**2**)

Compound **1** (13.00 g, 44.3 mmol) was dissolved in diphenylether (70 mL) and heated at 250 °C for 1 h. After cooling to rt, the mixture was filtered and the precipitates was washed with diphenylether (10 mL) and hexane (3 × 10 mL). The crude product was recrystallized from ethanol (150 mL); the solid was filtered and dried under reduced pressure to give **2** in 70% yield. ¹H NMR (400 MHz, DMSO-*d*₆): δ 11.92 (d, *J* = 3.8 Hz, 1H), 8.34 (d, *J* = 6.0 Hz, 1H), 7.70 (dd, *J*₁ = 1.9 Hz, *J*₂ = 7.5 Hz, 1H), 7.36–7.30 (m, 2H), 4.21 (q, *J* = 7.1 Hz, 2H), 4.00 (s, 3H), 1.27 (t, *J* = 7.1, 3H). ¹³C NMR (100 MHz, DMSO-*d*₆): δ 173.2, 164.2, 148.7, 144.0, 129.3, 128.1, 124.6, 116.7, 112.2, 110.0, 59.6, 56.3, 14.3. HRMS calcd for C₁₃H₁₃NNaO₄ 270.0737, found 270.0743.

5.3.3. Representative procedure for *N*-alkylation. Synthesis of ethyl 1-butyl-8-methoxy-4-oxo-1,4-dihydroquinoline-3-carboxylate (**3a**)

To a solution of **2** (0.28 g, 1.132 mmol) in DMF (5 mL) was added potassium carbonate (0.438 g, 3.17 mmol) and 1-bromobutane (0.340 mL, 3.17 mmol). The mixture was heated at 90 °C for 4 h, then cooled to rt and aq. HCl (0.2 M, 50 mL) was added. The mixture was extracted with CH₂Cl₂ (3 × 5 mL) and the combined organic

layers were dried over MgSO₄. Solvents were removed under reduced pressure and the residue was purified by silica gel chromatography using hexane:EtOAc (2:1) as eluent to give **3a** (0.33 g, 91% yield). ¹H NMR (400 MHz, CDCl₃): δ 9.14 (s, 1H), 7.83 (dd, *J*₁ = 1.1 Hz, *J*₂ = 8.5 Hz, 1H), 7.49 (t, *J* = 8.1 Hz, 1H), 7.13 (dd, *J*₁ = 0.8 Hz, *J*₂ = 7.8 Hz, 1H), 4.46 (q, *J* = 7.1 Hz, 2H), 4.23 (t, *J* = 6.6 Hz, 2H), 4.08 (s, 3H), 1.92–1.85 (m, 2H), 1.59–1.50 (m, 2H), 1.44 (t, *J* = 7.1 Hz, 3H), 0.99 (t, 7.4 Hz, 3H). ¹³C NMR (100 MHz, CDCl₃): δ 165.5, 164.0, 155.5, 150.8, 126.9, 124.9, 114.8, 114.7, 109.7, 76.1, 61.5, 56.1, 32.4, 19.2, 14.3, 13.9. HRMS calcd for C₁₇H₂₂NO₄ 304.1543, found 304.1541.

5.3.4. Ethyl 1-(2-ethoxyethyl)-8-methoxy-4-oxo-1,4-dihydroquinoline-3-carboxylate (**3b**)

3b was synthesized following the similar procedure as **3a** in 75% yield. ¹H NMR (400 MHz, CDCl₃): δ 9.19 (s, 1H), 7.96 (dd, *J*₁ = 1.0 Hz, *J*₂ = 8.5 Hz, 1H), 7.49 (t, *J* = 8.1 Hz, 1H), 7.13 (dd, *J*₁ = 0.7 Hz, *J*₂ = 7.6 Hz, 1H), 4.45 (q, *J* = 7.1 Hz, 2H), 4.40–4.38 (m, 2H), 4.08 (s, 3H), 3.85–3.83 (m, 2H), 3.57 (q, *J* = 7.0 Hz, 2H), 1.44 (t, *J* = 7.1 Hz, 3H), 1.20 (t, *J* = 7.0 Hz, 3H). ¹³C NMR (100 MHz, CDCl₃): δ 165.1, 164.1, 155.4, 150.8, 142.8, 126.9, 125.1, 115.2, 115.1, 109.8, 75.3, 69.6, 66.7, 61.5, 56.1, 15.1, 14.3. HRMS calcd for C₁₇H₂₂NO₅ 320.1492, found 320.1488.

5.3.5. Ethyl 1-(3-fluoropropyl)-8-methoxy-4-oxo-1,4-dihydroquinoline-3-carboxylate (**3c**)

3c was synthesized analogously as **3a** in 83% yield. ¹H NMR (400 MHz, CDCl₃): δ 9.20 (s, 1H), 7.80 (dd, *J*₁ = 1.1 Hz, *J*₂ = 8.5 Hz, 1H), 7.52 (t, *J* = 8.1 Hz, 1H), 7.15 (dd, *J*₁ = 0.8 Hz, *J*₂ = 7.8 Hz, 1H), 4.82 (t, *J* = 5.7 Hz, 1H), 4.70 (t, *J* = 5.7 Hz, 1H), 4.67 (q, *J* = 7.1 Hz, 2H), 4.37 (t, *J* = 6.1 Hz, 2H), 4.09 (s, 3H), 2.38–2.32 (m, 1H), 2.31–2.25 (m, 1H), 1.45 (t, *J* = 7.1 Hz, 3H). ¹³C NMR (100 MHz, CDCl₃): δ 150.8, 127.3, 114.5, 109.9, 81.3, 79.9, 71.8, 71.7, 61.7, 56.2, 31.4, 31.2, 14.2. HRMS calcd for C₁₆H₁₉FNO₄ 308.1293, found 308.1290.

5.3.6. Representative procedure for saponification. Synthesis of 1-butyl-8-methoxy-4-oxo-1,4-dihydroquinoline-3-carboxylic acid (**4a**)

Aq. NaOH (10%, 30 mL) was added to **3a** (0.33 g, 1.088 mmol) and the mixture was heated to reflux for 2 h. After the mixture was cooled to rt, the pH was adjusted to 2 using conc. HCl and the precipitates were collected and washed with water and diethylether. Recrystallization of the crude product from EtOH (50 mL) gave **4a** (0.278 g, 1.01 mmol, 93% yield). ¹H NMR (400 MHz, CDCl₃): δ 15.04 (s, 1H), 8.60 (s, 1H), 8.12 (dd, *J*₁ = 1.4 Hz, *J*₂ = 8.1 Hz, 1H), 7.50 (t, *J* = 8.0 Hz, 1H), 7.30 (dd, *J*₁ = 1.3 Hz, *J*₂ = 8.0 Hz, 1H), 4.62 (t, *J* = 7.6 Hz, 2H), 4.02 (s, 3H), 1.87–1.79 (m, 2H), 1.39 (t, *J* = 7.5 Hz, 2H), 0.97 (t, *J* = 7.4 Hz). ¹³C NMR (100 MHz, CDCl₃): δ 177.9, 167.2, 150.49, 150.3, 129.05, 126.6, 119.1, 115.5, 108.3, 60.5, 56.5, 33.5, 19.7, 13.7. HRMS calcd for C₁₅H₁₇NNaO₄ 298.1050, found 298.1047.

5.3.7. 1-(2-Ethoxyethyl)-8-methoxy-4-oxo-1,4-dihydroquinoline-3-carboxylic acid (**4b**)

4b was synthesized in an analogue way to **4a** in 85% yield. ¹H NMR (400 MHz, CDCl₃): δ 14.95 (s, 1H), 8.18 (dd, *J*₁ = 1.4 Hz, *J*₂ = 8.1 Hz, 1H), 7.49 (t, *J* = 8.1 Hz, 1H), 7.29 (dd, *J*₁ = 1.3 Hz, *J*₂ = 8.0 Hz, 1H), 4.82 (t, *J* = 4.9 Hz, 2H), 4.00 (s, 3H), 3.76 (t, *J* = 4.9 Hz, 2H), 3.40 (q, *J* = 7.0 Hz, 2H), 1.09 (t, *J* = 7.0 Hz, 3H). ¹³C NMR (100 MHz, CDCl₃): δ 152.0, 126.5, 119.3, 115.5, 69.0, 66.8, 59.9, 56.5, 15.0. HRMS calcd for C₁₅H₁₈NO₅ 192.1179, found 292.1175.

5.3.8. 1-(3-Fluoropropyl)-8-methoxy-4-oxo-1,4-dihydroquinoline-3-carboxylic acid (**4c**)

4c was obtained in the same way as **4a** in 55% yield. ¹H NMR (400 MHz, DMSO-*d*₆): δ 15.12 (s, 1H), 9.26 (s, 1H), 8.23 (dd,

$J_1 = 1.4$ Hz, $J_2 = 8.1$ Hz, 1H), 7.50 (t, $J = 8.1$ Hz, 1H), 7.20 (dd, $J_1 = 1.0$ Hz, $J_2 = 8.0$ Hz, 1H), 4.76 (t, $J = 5.5$ Hz, 1H), 4.65 (t, $J = 5.7$ Hz, 1H), 4.72 (t, $J = 7.4$ Hz, 2H), 4.52 (t, $J = 7.0$ Hz, 2H), 4.09 (s, 3H), 2.30–2.18 (m, 2H). ^{13}C NMR (100 MHz, DMSO- d_6): δ 178.2, 154.1, 126.5, 119.5, 115.3, 108.3, 81.3, 79.9, 72.0, 56.5, 52.9, 32.5. HRMS calcd for $\text{C}_{14}\text{H}_{15}\text{FNO}_4$ 280.0985, found 280.0982.

5.3.9. Synthesis of 3-hydroxy-1-aminoadamantane (5)

To an ice-cooled mixture of sulfuric acid (96%, 12.33 mL, 231 mmol) and nitric acid (65%, 1.2 mL, 26.5 mmol) was added 1-aminoadamantane hydrochloride (1 g, 6.61 mmol) portion wise. The mixture was stirred at rt for 2 days, ice-water (6 mL) was added to the reaction mixture. The solution was stirred in an ice-water bath for 30 min; KOH (35 g, 0.62 mol) was added in small portions over 1 h at such a rate to keep the temperature below 80 °C. The resulting white paste was mixed with CH_2Cl_2 (300 mL) and vigorously stirred for 1 h. The solid was filtered off, and the mother liquor was evaporated to dryness under reduced pressure to provide **5** (527 mg, 3.15 mmol) in 48% yield as a white solid. ^1H NMR (400 MHz, DMSO- d_6): δ 4.33 (s, 1H), 2.08 (s, 2H), 1.49–1.42 (m, 5H), 1.38–1.35 (m, 9H). ^{13}C NMR (100 MHz, DMSO- d_6): δ 67.7, 54.0, 44.8, 44.1, 34.8, 30.5. HRMS calcd for $\text{C}_{10}\text{H}_{18}\text{NO}$ 168.1383, found 168.1380.

5.3.10. Representative procedure for amide formation. Synthesis of *N*-(1-adamantyl)-1-butyl-8-methoxy-4-oxo-1,4-dihydroquinoline-3-carboxamide (RS-005)

To a suspension of **3a** (206 mg, 0.748 mmol) in DMF (10 mL) was added DIPEA (0.392 mL, 2.245 mmol) and the solution was stirred at rt for 30 min. HBTU (568 mg, 1.497 mmol) was added portion wise, followed by the addition of 1-aminoadamantane (0.136 g, 0.898 mmol). The mixture was stirred at rt for 4 h and diluted with EtOAc (60 mL), washed with water (3 x 10 mL), HCl (0.5 M, 10 mL), water (10 mL) and brine (15 mL). Solvents were removed under reduced pressure and the residue was purified with flash chromatography using hexane:EtOAc (10:1 to 2:1) to give **RS-005** (263 mg, 0.644 mmol, 86% yield). ^1H NMR (400 MHz, CDCl_3): δ 9.95 (s, 1H), 8.63 (s, 1H), 8.16 (dd, $J_1 = 1.4$ Hz, $J_2 = 8.2$ Hz, 1H), 7.38 (t, $J = 8.0$ Hz, 1H), 7.18 (dd, $J_1 = 1.3$ Hz, $J_2 = 8.0$ Hz, 1H), 4.54 (t, $J = 7.6$ Hz, 2H), 3.98 (s, 3H), 2.19–2.11 (m, 9H), 1.83–1.68 (m, 8H), 1.37 (m, $J = 7.5$ Hz, 2H), 0.95 (t, $J = 7.4$ Hz, 3H). ^{13}C NMR (100 MHz, CDCl_3): δ 149.8, 125.1, 119.3, 114.1, 59.7, 56.3, 51.6, 41.8, 36.6, 33.5, 29.6, 19.8, 13.7. HRMS calcd for $\text{C}_{25}\text{H}_{33}\text{N}_2\text{O}_3$ 409.2486, found 409.2492.

5.3.11. *N*-(tert-butyl)-1-butyl-8-methoxy-4-oxo-1,4-dihydroquinoline-3-carboxamide (RS-006)

RS-006 was prepared in the same way as **RS-005** in 92% yield. ^1H NMR (400 MHz, CDCl_3): δ 10.05 (s, 1H), 8.64 (s, 1H), 8.14 (dd, $J_1 = 1.4$ Hz, $J_2 = 8.2$ Hz, 1H), 7.37 (t, $J = 7.9$ Hz, 1H), 7.18–7.17 (m, 1H), 4.53 (t, $J = 6.3$ Hz, 2H), 3.96 (s, 3H), 1.79 (m, 2H), 1.48 (s, 9H), 1.36 (m, 2H), 0.94 (t, $J = 7.4$ Hz, 3H). ^{13}C NMR (100 MHz, CDCl_3): δ 149.8, 125.2, 119.2, 114.2, 59.7, 56.3, 33.5, 29.0, 19.8, 13.7. HRMS calcd for $\text{C}_{19}\text{H}_{27}\text{N}_2\text{O}_3$ 331.2016, found 331.2018.

5.3.12. 1-Butyl-*N*-cyclopentyl-8-methoxy-4-oxo-1,4-dihydroquinoline-3-carboxamide (RS-007)

RS-007 was obtained in the same way as **RS-005** in 90% yield. ^1H NMR (400 MHz, CDCl_3): δ 10.00 (s, 1H), 8.67 (s, 1H), 8.13 (dd, $J_1 = 1.4$ Hz, $J_2 = 8.2$ Hz, 1H), 7.39 (t, $J = 8.0$ Hz, 1H), 7.20–7.18 (m, 1H), 4.56 (t, $J = 7.5$ Hz, 2H), 4.40 (m, $J = 6.8$ Hz, 1H), 3.96 (s, 3H), 2.07–1.98 (m, 2H), 1.81–1.73 (m, 4H), 1.64–1.57 (m, 4H), 1.36 (m, $J = 7.5$ Hz, 2H), 0.93 (t, $J = 7.4$ Hz, 3H). ^{13}C NMR (100 MHz, CDCl_3): δ 150.1, 149.8, 130.3, 125.4, 119.1, 114.4, 59.8, 56.3, 50.9, 33.5, 33.2, 23.9, 19.7, 13.7. HRMS calcd for $\text{C}_{20}\text{H}_{27}\text{N}_2\text{O}_3$ 343.2016, found 343.2016.

5.3.13. 1-Butyl-*N*-(cyclopropylmethyl)-8-methoxy-4-oxo-1,4-dihydroquinoline-3-carboxamide (RS-008)

RS-008 was obtained in a similar way to **RS-005** in 89% yield. ^1H NMR (400 MHz, CDCl_3): δ 10.11 (s, 1H), 8.67 (s, 1H), 8.18 (dd, $J_1 = 1.4$ Hz, $J_2 = 8.2$ Hz, 1H), 7.40 (t, $J = 8.0$ Hz, 1H), 7.21–7.19 (m, 1H), 4.57 (t, $J = 7.3$ Hz, 2H), 3.98 (s, 3H), 3.35–3.32 (m, 2H), 1.83–1.76 (m, 2H), 1.37 (m, $J = 7.5$ Hz, 2H), 1.15–1.05 (m, 1H), 0.95 (s, $J = 7.4$, 3H), 0.57–0.52 (m, 2H), 0.31–0.27 (m, 2H). ^{13}C NMR (100 MHz, CDCl_3): δ 150.0, 125.3, 119.3, 114.3, 59.7, 56.3, 44.0, 33.5, 19.8, 13.7, 10.9, 3.5. HRMS calcd for $\text{C}_{19}\text{H}_{25}\text{N}_2\text{O}_3$ 329.1860, found 329.1859.

5.3.14. *N*-(tert-butyl)-1-(3-fluoropropyl)-8-methoxy-4-oxo-1,4-dihydroquinoline-3-carboxamide (RS-011)

RS-011 was synthesized as an analogue of **RS-005** in 81% yield. ^1H NMR (400 MHz, CDCl_3): δ 10.00 (s, 1H), 8.67 (s, 1H), 8.16 (dd, $J_1 = 1.4$ Hz, $J_2 = 8.1$ Hz, 1H), 7.40 (t, $J = 8.0$ Hz, 1H), 7.20 (dd, $J_1 = 1.3$ Hz, $J_2 = 8.0$ Hz, 1H), 4.72 (t, $J = 7.4$ Hz, 2H), 4.57 (t, $J = 5.5$ Hz, 1H), 4.46 (t, $J = 5.5$ Hz, 1H), 3.98 (s, 3H), 2.30–2.17 (m, 2H), 1.49 (s, 9H). ^{13}C NMR (CDCl_3): δ = 149.8, 130.6, 125.4, 119.3, 114.2, 81.5, 79.9, 56.2, 50.9, 32.5, 29.0. ^{19}F NMR (CDCl_3): δ = -222.04 (m). HRMS calcd for $\text{C}_{18}\text{H}_{24}\text{FN}_2\text{O}_3$ 335.1765, found 335.1763.

5.3.15. *N*-(1-adamantyl)-1-(2-ethoxyethyl)-8-methoxy-4-oxo-1,4-dihydroquinoline-3-carboxamide (RS-016)

RS-016 was prepared in the same way as **RS-005** in 75% yield. ^1H NMR (400 MHz, CHCl_3): δ 9.91 (s, 1H), 8.66 (s, 1H), 8.17 (dd, $J_1 = 1.4$ Hz, $J_2 = 8.2$ Hz, 1H), 7.38 (t, $J_1 = 8.0$ Hz), 7.18 (t, $J_1 = 1.2$ Hz, $J_2 = 8.0$ Hz, 1H), 4.73 (t, $J = 5.5$ Hz, 2H), 3.96 (s, 3H), 3.75 (t, $J = 5.5$ Hz, 2H), 3.41 (q, $J = 7.0$ Hz, 2H), 2.18 (s, 6H), 2.11 (s, 3H), 1.77–1.68 (m, 6H), 1.11 (t, $J = 7.0$ Hz, 3H). ^{13}C NMR (100 MHz, CDCl_3): δ 151.1, 125.2, 119.6, 114.4, 69.7, 66.9, 59.0, 56.5, 42.0, 36.8, 29.7. HRMS calcd for $\text{C}_{25}\text{H}_{34}\text{N}_2\text{O}_4$ 425.2436, found 425.2436.

5.3.16. 1-(2-Ethoxyethyl)-8-methoxy-4-oxo-*N*-phenethyl-1,4-dihydroquinoline-3-carboxamide (RS-022)

RS-022 was obtained in a similar way as **RS-005** in 69% yield. ^1H NMR (400 MHz, DMSO- d_6): δ 9.96 (t, $J = 5.7$ Hz, 1H), 8.61 (s, 1H), 7.98–7.93 (m, 1H), 7.49–7.44 (m, 2H), 7.32–7.26 8 (m, 4H), 7.23–7.18 (m, 1H), 4.82 (t, $J = 4.8$ Hz, 2H), 3.95 (s, 3H), 3.69 (t, $J = 4.8$ Hz, 2H), 3.60–3.55 (m, 2H), 3.35 (q, $J = 7.0$ Hz, 2H), 2.85 (t, $J = 7.2$ Hz, 2H), 0.97 (t, $J = 7.0$ Hz, 3H). ^{13}C NMR (100 MHz, DMSO- d_6): δ 151.2, 128.6, 128.3, 126.1, 125.5, 118.1, 115.4, 68.7, 65.5, 58.3, 56.7, 35.4, 14.9. HRMS calcd for $\text{C}_{23}\text{H}_{27}\text{N}_2\text{O}_4$ 395.1965, found 395.1964.

5.3.17. 1-(2-Ethoxyethyl)-*N*-(3-hydroxyadamantan-1-yl)-8-methoxy-4-oxo-1,4-dihydroquinoline-3-carboxamide (RS-028)

RS-028 was prepared in a similar way as **RS-005** in 84% yield. ^1H NMR (400 MHz, CDCl_3): δ 10.04 (s, 1H), 8.64 (s, 1H), 8.16 (dd, $J_1 = 1.4$ Hz, $J_2 = 8.1$ Hz, 1H), 7.39 (t, $J = 8.0$ Hz, 1H), 7.19 (dd, $J_1 = 1.2$ Hz, $J_2 = 8.0$ Hz, 1H), 4.74 (t, $J = 5.4$ Hz, 2H), 3.97 (s, 3H), 3.75 (t, $J = 5.4$ Hz, 2H), 3.42 (q, $J = 7.0$ Hz, 2H), 2.31–2.04 (m, 9H), 1.78–1.62 (m, 5H), 1.42 (s, 1H), 1.11 (t, $J = 7.0$ Hz, 3H). ^{13}C NMR (100 MHz, CDCl_3): δ 150.9, 114.3, 69.5, 59.0, 56.3, 49.3, 44.2, 40.5, 35.1, 30.7. HRMS calcd for $\text{C}_{25}\text{H}_{33}\text{N}_2\text{O}_5$ 441.2384, found 441.2382.

5.3.18. Synthesis of *N*-(1-adamantyl)-1-(2-ethoxyethyl)-8-hydroxy-4-oxo-1,4-dihydroquinoline-3-carboxamide (6)

To a solution of **RS-016** (202 mg, 0.476 mmol) in DMF (5 mL) was added lithium chloride (303 mg, 7.14 mmol). The mixture was heated to reflux and stirred overnight, then cooled to rt. Ethyl acetate (EtOAc, 60 mL) was added and the mixture was washed with HCl (0.2 M, 3 x 10 mL) and brine (15 mL). The organic layer was dried over MgSO_4 and solvent was removed under reduced pressure. The residue was purified by HPLC with a C18 column using

0.1% TFA in water and acetonitrile (30:70) as eluent to afford the desired product **6** (37 mg, 0.090 mmol, 20% yield). ^1H NMR (400 MHz, CDCl_3): δ 10.00 (s, 1H), 8.65 (s, 1H), 8.33 (br s, 1H), 8.14 (dd, $J_1 = 2.5$ Hz, $J_2 = 7.1$ Hz, 1H), 7.35–7.29 (m, 2H), 4.75 (t, $J = 4.9$ Hz, 2H), 4.00 (t, $J = 4.9$ Hz, 2H), 3.61 (q, $J = 7.0$ Hz, 2H), 2.14–2.09 (m, 3H), 1.78–1.67 (m, 12H), 1.18 (t, $J = 7.0$ Hz, 3H). ^{13}C NMR (100 MHz, CDCl_3): δ 149.11, 125.62, 123.36, 119.80, 69.37, 67.81, 55.34, 41.76, 36.53, 31.93, 29.70, 29.53, 29.36, 14.62. HRMS calcd for $\text{C}_{24}\text{H}_{31}\text{N}_2\text{O}_4$ (M + H) 411.2278, found 411.2281.

5.4. *In vitro* binding assay

Competitive binding reactions were initiated by the addition of a membrane preparation obtained from CHO–K1 cells stably transfected with human CB1 and CB2, respectively, from PerkinElmer (0.5 $\mu\text{g}/\text{tube}$ for hCB1 and hCB2) into incubation tubes. [^3H]CP-55,940 (1.4 nM) was used as the radioligand. Six to 10 concentrations (ranging from 1 pM to 10 μM) of displacing ligand (compound to be tested) in assay buffer (50 mM TRIS, 1 mM EDTA, 3 mM MgCl_2 and 0.05% bovine serum albumin, pH adjusted to 7.4) were added. Nonspecific binding was defined by the presence of hCB1/hCB2 agonist 5 μM WIN-55212-2 (K_i 1.89 and 0.28 nM, respectively) [32]. After incubation at 30 °C for 90 min, reactions were terminated by the addition of ice cold assay buffer (3 mL) followed by rapid vacuum filtration through a Whatman GF/C filter (pre-soaked for 2 h in 0.05% polyethylenimine in water) and washed twice with ice cold assay buffer (3 mL). The bound activity was counted in a Beckman LS 6500 Liquid Scintillation Counter after adding 3 mL scintillation cocktail (Ultima Gold, Perkin Elmer) and thorough shaking. For each mean value three experiments, each in triplicates, were performed. Inhibition constants (K_i) were determined from the IC_{50} values using the Cheng–Prusoff equation [33]. For calculations, K_D values of 0.14 and 0.11 nM from PerkinElmer were used for [^3H]CP-55,940 binding to hCB1 and hCB2 receptors, respectively.

5.5. Radiochemistry

[^{11}C]CO $_2$ was produced via the $^{14}\text{N}(p,\alpha)^{11}\text{C}$ nuclear reaction by bombardment of nitrogen gas fortified with 0.5% oxygen using a Cyclone 18/9 cyclotron (18-MeV; IBA, Belgium). After reduction over a supported nickel catalyst to [^{11}C]CH $_4$ and subsequent gas phase iodination, [^{11}C]CH $_3\text{I}$ was bubbled through a mixture of precursor **6** (1 mg) and cesium carbonate (5 mg) in DMF (0.6 mL). The mixture was heated at 90 °C for 3 min. After dilution with water (1.4 mL), the crude product was purified using the semi-preparative HPLC system (product peak at 9.1 min). The collected product was diluted with water (10 mL), trapped on a C18 cartridge (Waters, preconditioned with 5 mL EtOH and 10 mL water), washed with water (5 mL) and eluted with EtOH (0.5 mL). For formulation of the final product [^{11}C]RS-016, water for injection (9.5 mL) was added to give an ethanol concentration of 5%. For quality control, an aliquot of the formulated solution was injected into the analytical HPLC system. The identity of the ^{11}C -labeled product was confirmed by comparison with the retention time of its nonradioactive reference compound RS-016 (10.64 min) and by co-injection. Specific activity of [^{11}C]RS-016 was calculated by comparison of UV peak intensity with a calibration curve of the cold reference compound.

5.6. *In vitro* autoradiography

Rodent spleen or brain and human spinal cord tissue (post mortem autopsy material from ALS patients, ALS Clinic, Kantonsspital St. Gallen, Switzerland) were embedded in TissueTek and cut into 20 μm -thick sections on a Cryostat HM 505 N (Microm) at

–15 °C (blade and block). The slices were absorbed on SuperFrost Plus slides (Menzel) and stored at –80° until use. For the experiment, the slices were thawed on ice for 10 min before conditioning in incubation buffer (50 mM TRIS/HCl, 5% BSA, pH 7.4) on ice for 10 min. Excess solution was carefully removed and the tissue slices were dried in a ventilated hood for 10 min. The slices were incubated with [^{11}C]RS-016 (600 μL , 0.2 nM in incubation buffer) for 15 min at rt in a humid chamber. For blockade conditions, the slices were dripped with 600 μL of a mixture of radioligand and GW405833 (5 μM). After incubation, the slices were washed with washing buffer (50 mM TRIS/HCl, 1% BSA, 5% EtOH, pH 7.4) for 2 min (2 \times) and with distilled water for 5 s (2 \times) on ice. After drying for 10 min at rt, the slices were exposed (30 min) to phosphor imager plates (Fuji) and the films were scanned in a BAS5000 reader (Fuji).

5.7. *In vitro* stability

The tracer stability was examined *in vitro* in rodent plasma (mouse and rat) and human plasma at time points 5', 10', 15' and 20'. Plasma (400 μL) was incubated with 10 μL of [^{11}C]RS-016 formulated solution at 37 °C under shaking. At each time point, an aliquot (100 μL) of the mixture was collected and the reaction stopped with 100 μL ice-cooled CH_3CN . The samples were centrifuged (3 min, 5000 rpm) and the supernatant collected. Each sample was analyzed by radio-TLC Instant Imager (Packard, Canberra Company) using hexane:EtOAc (1:1).

5.8. Determination of $\log D_{7.4}$

The partition coefficient D was determined by the shake-flask method as reported in Ref. [34]. In brief, n-octanol saturated with phosphate buffer pH 7.4 (0.5 mL) and phosphate buffer saturated with n-octanol (0.5 mL) were mixed with [^{11}C]RS-016 (20 μL) formulated solution. The samples were shaken for 15 min and then centrifuged at 5000 g for 5 min. Radioactivities in each phase was measured in a gamma counter (Wizard, PerkinElmer). $\log D$ is expressed as the logarithm of the ratio between the radioactivity concentrations (Bq/mL) of the octanol and the buffer phase.

5.9. *In vivo* metabolite studies

In vivo stability and metabolite studies were performed in healthy Wistar rats. Radiotracer solution (115–163 MBq, 0.24–0.34 nmol) was injected *via* tail vein and blood was collected at three different time points (5', 10' 20' min). After 20 min the rats were sacrificed, urine was collected and spleen was removed. Plasma was separated from the blood cells by centrifugation at 5000 g for 5 min at 4 °C. Proteins of plasma and urine were precipitated by centrifugation with ice-cold CH_3CN . The spleen tissue was homogenated in PBS (2 mL), extracted with cold CH_3CN and centrifuged. Supernatants were analyzed by radio-TLC using hexane:EtOAc (1:1). Results are expressed as percentage of total activity.

5.10. Biodistribution studies

For biodistribution studies in male Wistar rats, [^{11}C]RS-016 (5–10 MBq, 0.01–0.02 nmol) were administered *via* tail vein injection into Wistar rats ($n = 3$). For blocking studies, GW405833 (1.5 mg/kg) was injected sc 30 min before the experiment ($n = 3$). Animals were sacrificed under anesthesia with isoflurane by decapitation at 15 min p.i. Organs were collected, weighed and radioactivity measured in a gamma-counter. The accumulated radioactivity in the organs was expressed as percent normalized injected dose per gram of tissue (normalized %ID/g tissue).

5.11. Tissue preparation, RNA isolation and quantitative real-time PCR

Mice were sacrificed 0, 3 and 5 days after ip injection of 10 mg/kg lipopolysaccharide or vehicle (saline). Whole brain and spleen were dissected and immediately frozen in liquid nitrogen and stored at -80°C until use. Total RNA was extracted as previously reported [35]. Quantification of the RNA was done by spectrophotometric analysis. QuantiTect[®] Reverse Transcription Kit (Qiagen, Hilden, Germany) was used to generate cDNA. Quantitative polymerase chain reaction (qPCR) was performed with the following primers (Microsynth, Balgach, Switzerland), mouse *CNR2*: forward 5'-CTACAAAGCTCTAGTCACCCGT-3', reverse 5'-CCATGAGCGG-CAGGTAAGAAA-3'; mouse beta-actin (*ACTB*): forward 5'-AGACCTCTATGCCAACACAGT-3', reverse 5'-TGCTAGGAGCCA-GAGCAGTAA-3' and with the DyNAmo[™] Flash SYBR[®] Green qPCR Kit (Thermo Scientific) using a 7900 HT Fast Real-Time PCR System (Applied Biosystems, Carlsbad, CA, USA). All reactions were performed in duplicates and in three independent runs. Quantitative analysis was calculated as previously reported [35].

5.12. In vivo PET

For small animal PET brain scans, animals were anesthetized with isoflurane and [¹¹C]RS-016 (10–18 MBq, 0.02–0.04 nmol) were injected *via* the tail vein. For blocking conditions, 2.0 mg/kg GW405833 was injected sc 30 min before tracer application. Depth of anesthesia was monitored by measuring respiratory frequency (SA Instruments, Inc., Stony Brook, USA). Body temperature was controlled by a rectal probe and kept at 37°C by a thermocoupler and a heated air stream. Data were reconstructed in user-defined time frames with a voxel size of $0.3875 \times 0.3875 \times 0.775 \text{ mm}^3$ by 2-dimensional-ordered subsets expectation maximization (2D-OSEM). Random and single but no attenuation correction was applied. PET acquisitions were followed by a CT for anatomical orientation. Image files were analyzed with PMOD 3.5 software (PMOD Technologies Ltd., Zurich, Switzerland). Time activity curves (TACs) based on the regions of interest (ROI) defined on the mouse MRI T2 template were calculated. Tissue radioactivity of brain ROI were expressed as standardized uptake values (SUV), that is, the decay-corrected radioactivity per cm^3 divided by the injected radioactivity dose per gram of body weight.

5.13. Statistics

Quantitative PCR data are given as mean values with standard deviations and analyzed by one way analysis of variance (ANOVA) tests, followed by corrections for multiple post-hoc tests (Holm–Sidak, Bonferroni). Time activity curves were compared by two-tailed homoscedastic Student's t-test.

Conflict of interest

The authors declare no conflict interest.

Acknowledgments

We thank Mr. Bruno Mancosu for his support with carbon-11 radiolabeling and Mrs. Claudia Keller for performing PET/CT scans. We also thank the Swiss ALS Foundation (2-70664-14) for partly financing this project.

Appendix A. Supplementary data

Supplementary data related to this article can be found at <http://dx.doi.org/10.1016/j.ejmech.2015.01.028>.

dx.doi.org/10.1016/j.ejmech.2015.01.028.

References

- [1] L.A. Matsuda, S.J. Lolait, M.J. Brownstein, A.C. Young, T.I. Bonner, Structure of a cannabinoid receptor and functional expression of the cloned cDNA, *Nature* 346 (1990) 561–564.
- [2] S. Munro, K.L. Thomas, M. Abu-Shaar, Molecular characterization of a peripheral receptor for cannabinoids, *Nature* 365 (1993) 61–65.
- [3] K. Mackie, Distribution of cannabinoid receptors in the central and peripheral nervous system, *Handb. Exp. Pharmacol.* (2005) 299–325.
- [4] M.K. Sharma, P.R. Murumkar, A.M. Kanhed, R. Giridhar, M.R. Yadav, Prospective therapeutic agents for obesity: molecular modification approaches of centrally and peripherally acting selective cannabinoid 1 receptor antagonists, *Eur. J. Med. Chem.* 79 (2014) 298–339.
- [5] M.D. Van Sickle, M. Duncan, P.J. Kingsley, A. Mouihate, P. Urbani, et al., Identification and functional characterization of brainstem cannabinoid CB2 receptors, *Science* 310 (2005) 329–332.
- [6] J.C. Ashton, D. Friberg, C.L. Darlington, P.F. Smith, Expression of the cannabinoid CB2 receptor in the rat cerebellum: an immunohistochemical study, *Neurosci. Lett.* 396 (2006) 113–116.
- [7] A. Brusco, P. Tagliaferro, T. Saez, E.S. Onaivi, Postsynaptic localization of CB2 cannabinoid receptors in the rat hippocampus, *Synapse* 62 (2008) 944–949.
- [8] C. Benito, R.M. Tolon, M.R. Pazos, E. Nunez, A.I. Castillo, J. Romero, Cannabinoid CB2 receptors in human brain inflammation, *Br. J. Pharmacol.* 153 (2008) 277–285.
- [9] E.S. Onaivi, Cannabinoid receptors in brain: pharmacogenetics, neuropharmacology, neurotoxicology, and potential therapeutic applications, *Int. Rev. Neurobiol.* 88 (2009) 335–369.
- [10] J.L. Shoemaker, K.A. Seely, R.L. Reed, J.P. Crow, P.L. Prather, The CB2 cannabinoid agonist AM-1241 prolongs survival in a transgenic mouse model of amyotrophic lateral sclerosis when initiated at symptom onset, *J. Neurochem.* 101 (2007) 87–98.
- [11] Y. Yiangou, P. Facer, P. Durrenberger, I.P. Chessell, A. Naylor, et al., COX-2, CB2 and P2X7-immunoreactivities are increased in activated microglial cells/macrophages of multiple sclerosis and amyotrophic lateral sclerosis spinal cord, *BMC Neurol.* 6 (2006) 12.
- [12] D.R. Rosen, Mutations in Cu/Zn superoxide dismutase gene are associated with familial amyotrophic lateral sclerosis, *Nature* 364 (1993) 362.
- [13] L. Zinman, M. Cudkowicz, Emerging targets and treatments in amyotrophic lateral sclerosis, *Lancet Neurol.* 10 (2011) 481–490.
- [14] D.J. Graber, W.F. Hickey, B.T. Harris, Progressive changes in microglia and macrophages in spinal cord and peripheral nerve in the transgenic rat model of amyotrophic lateral sclerosis, *J. Neuroinflamm.* 7 (2010) 8.
- [15] L.G. Bilsland, The endocannabinoid system in amyotrophic lateral sclerosis, *Curr. Pharm. Des.* 14 (2006) 2306–2316.
- [16] V. Lucchesi, T. Parkkari, J.R. Savinainen, A.M. Malfitano, M. Allara, et al., 1,2-Dihydro-2-oxopyridine-3-carboxamides: the C-5 substituent is responsible for functionality switch at CB2 cannabinoid receptor, *Eur. J. Med. Chem.* 74 (2014) 524–532.
- [17] R. Ahmad, M. Koole, N. Evens, K. Serdons, A. Verbruggen, et al., Whole-body biodistribution and radiation dosimetry of the cannabinoid type 2 receptor ligand [C]-NE40 in healthy subjects, *Mol. Imaging Biol.* 15 (2013) 384–390.
- [18] L. Mu, D. Bieri, R. Slavik, K. Drandarov, A. Muller, et al., Radiolabeling and in vitro/in vivo evaluation of N-(1-adamantyl)-8-methoxy-4-oxo-1-phenyl-1,4-dihydroquinoline-3-carboxamide as a PET probe for imaging cannabinoid type 2 receptor, *J. Neurochem.* 126 (2013) 616–624.
- [19] N. Evens, G.G. Muccioli, N. Houbrechts, D.M. Lambert, A.M. Verbruggen, et al., Synthesis and biological evaluation of carbon-11- and fluorine-18-labeled 2-oxoquinoline derivatives for type 2 cannabinoid receptor positron emission tomography imaging, *Nucl. Med. Biol.* 36 (2009) 455–465.
- [20] A.G. Horti, Y. Gao, H.T. Ravert, P. Finley, H. Valentine, et al., Synthesis and biodistribution of [¹¹C]A-836339, a new potential radioligand for PET imaging of cannabinoid type 2 receptors (CB2), *Bioorg. Med. Chem.* 18 (2010) 5202–5207.
- [21] N. Evens, C. Vandeputte, G.G. Muccioli, D.M. Lambert, V. Baekelandt, et al., Synthesis, in vitro and in vivo evaluation of fluorine-18 labelled FE-GW405833 as a PET tracer for type 2 cannabinoid receptor imaging, *Bioorg. Med. Chem.* 19 (2011) 4499–4505.
- [22] C. Vandeputte, N. Evens, J. Toelen, C.M. Deroose, B. Bosier, et al., A PET brain reporter gene system based on type 2 cannabinoid receptors, *J. Nucl. Med.* 52 (2011) 1102–1109.
- [23] T. Ruhl, W. Deuther-Conrad, S. Fischer, R. Gunther, L. Hennig, et al., Cannabinoid receptor type 2 (CB2)-selective N-aryl-oxadiazolyl-propionamides: synthesis, radiolabelling, molecular modelling and biological evaluation, *Org. Med. Chem. Lett.* 2 (2012) 32.
- [24] L. Hortalá, J. Arnaud, P. Roux, D. Oustric, L. Boulu, et al., Synthesis and preliminary evaluation of a new fluorine-18 labelled triazine derivative for PET imaging of cannabinoid CB2 receptor, *Bioorg. Med. Chem. Lett.* 24 (2014) 283–287.
- [25] S. Pasquini, A. Ligresti, C. Mugnaini, T. Semeraro, L. Cicione, et al., Investigations on the 4-quinolone-3-carboxylic acid motif. 3. Synthesis, structure-affinity relationships, and pharmacological characterization of 6-substituted 4-quinolone-3-carboxamides as highly selective cannabinoid-2

- receptor ligands, *J. Med. Chem.* 53 (2010) 5915–5928.
- [26] U. Hassiepen, M. Kittelmann, Adamantyl o-glucuronide derivatives as inhibitors of dipeptidyl peptidase iv for the threatment of diabetes, WO2005012249 (A2) (2005) 1–68.
- [27] R.N. Waterhouse, Determination of lipophilicity and its use as a predictor of blood-brain barrier penetration of molecular imaging agents, *Mol. Imaging Biol.* 5 (2003) 376–389.
- [28] H. Pajouhesh, G.R. Lenz, Medicinal chemical properties of successful central nervous system drugs, *NeuroRx* 2 (2005) 541–553.
- [29] K.J. Valenzano, L. Tafesse, G. Lee, J.E. Harrison, J.M. Boulet, et al., Pharmacological and pharmacokinetic characterization of the cannabinoid receptor 2 agonist, GW405833, utilizing rodent models of acute and chronic pain, anxiety, ataxia and catalepsy, *Neuropharmacology* 48 (2005) 658–672.
- [30] S. Galiegue, S. Mary, J. Marchand, D. Dussosoy, D. Carriere, et al., Expression of central and peripheral cannabinoid receptors in human immune tissues and leukocyte subpopulations, *Eur. J. Biochem.* 232 (1995) 54–61.
- [31] L. Qin, X. Wu, M.L. Block, Y. Liu, G.R. Breese, et al., Systemic LPS causes chronic neuroinflammation and progressive neurodegeneration, *Glia* 55 (2007) 453–462.
- [32] V.M. Showalter, D.R. Compton, B.R. Martin, M.E. Abood, Evaluation of binding in a transfected cell line expressing a peripheral cannabinoid receptor (CB2): identification of cannabinoid receptor subtype selective ligands, *J. Pharmacol. Exp. Ther.* 278 (1996) 989–999.
- [33] Y. Cheng, W.H. Prusoff, Relationship between the inhibition constant (K₁) and the concentration of inhibitor which causes 50 per cent inhibition (I₅₀) of an enzymatic reaction, *Biochem. Pharmacol.* 22 (1973) 3099–3108.
- [34] A.A. Wilson, L. Jin, A. Garcia, J.N. DaSilva, S. Houle, An admonition when measuring the lipophilicity of radiotracers using counting techniques, *Appl. Radiat. Isot.* 54 (2001) 203–208.
- [35] A. Müller, L. Mu, R. Meletta, K. Beck, Z. Rancic, et al., Towards non-invasive imaging of vulnerable atherosclerotic plaques by targeting co-stimulatory molecules, *Int. J. Cardiol.* 174 (2014) 503–515.